# Stoichiometric engineering of chalcogenide semiconductor alloys for nanophotonic applications

Piccinotti, Davide; Gholipour, Behrad; Yao, Jin; MacDonald, Kevin F.; Hayden, Brian E.; Zheludev, Nikolay I.

2019

Piccinotti, D., Gholipour, B., Yao, J., MacDonald, K. F., Hayden, B. E., & Zheludev, N. I. (2019). Stoichiometric Engineering of Chalcogenide Semiconductor Alloys for Nanophotonic Applications. Advanced Materials, 31(14), 1807083-. doi:10.1002/adma.201807083

https://hdl.handle.net/10356/144736

https://doi.org/10.1002/adma.201807083

# Stoichiometric Engineering of Chalcogenide Semiconductor Alloys for Nanophotonic Applications

*Davide Piccinotti*, Behrad Gholipour*, Jin Yao, Kevin F. MacDonald, Brian E. Hayden and Nikolay I. Zheludev*

D. Piccinotti, Dr. B. Gholipour, Prof. K. F. MacDonald, and Prof. N. I. Zheludev
Optoelectronics Research Centre and Centre for Photonic Metamaterials, University of Southampton, Southampton, SO17 1BJ, UK
E-mail: dp5c14@soton.ac.uk, b.gholipour@soton.ac.uk

Dr. B. Gholipour, Dr. J. Yao, and Prof. B. E. Hayden
Department of Chemistry, University of Southampton, Southampton, SO17 1BJ, UK

Prof. N. I. Zheludev
Centre for Disruptive Photonic Technologies & The Photonics Institute, School of Physical and Mathematical Sciences, Nanyang Technological University, Singapore 637371

Keywords: plasmonics, nanophotonics, metamaterials, chalcogenides, high-throughput

A variety of alternative plasmonic and dielectric material platforms – among them nitrides, semiconductors and conductive oxides - have come to prominence in recent years as means to address the shortcomings of noble metals (including Joule losses, cost, passive character) in certain nanophotonic and optical frequency metamaterial applications. Here, we show chalcogenide semiconductor alloys offer a uniquely broad pallet of optical properties, complementary to those of existing material platforms, which can be controlled by stoichiometric design. Using combinatorial high-throughput techniques, we explore the extraordinary epsilon-near-zero, plasmonic and low/high-index characteristics of Bi:Sb:Te (BST) alloys: Depending upon composition they can for example: have plasmonic figures of merit higher than conductive oxides and nitrides across the entire UV-NIR range, and higher than gold below 550 nm; present dielectric figures of merit better than conductive oxides at near-infrared telecommunications wavelengths; and exhibit record-breaking refractive indices as low as 0.7 and as high as 11.5.

Nanophotonics and photonic metamaterials research is driving the development of a variety of innovative devices showing unprecedented functionalities such as subwavelength waveguides and switches, optical nanoantennas, superlenses, optical invisibility cloaks, hyperlenses and light concentrators.[1, 2] These artificial electromagnetic media are engineered by structuring plasmonic metals or high-index dielectrics on the subwavelength scale. In recent years, 'all-dielectric' metamaterials and metasurfaces have been extensively studied as alternatives to their plasmonic counterparts for a variety of reasons:[3-5] high optical frequency absorption losses in noble metals constrain the performance of plasmonic metamaterials in certain applications, [6, 7] as can their relatively low melting points; such metals are also not compatible with established complementary metal oxide semiconductor (CMOS) manufacturing processes for optoelectronic devices, and their optical properties are neither compositionally adjustable nor particularly responsive to external excitations (as is desirable for the realization of 'active' – dynamically switchable or tuneable, and nonlinear photonic functionalities).

As such, there is considerable ongoing interest in the identification of alternative material platforms for plasmonic and photonic metamaterial applications. Investigations have variously encompassed conductive oxides, nitrides, [8] superconductors[9] and graphene[10], to name but a few.[11] Among candidate materials, chalcogenides (alloys containing at least one of the 'chalcogen' elements sulphur, selenium or tellurium) are perhaps the most versatile: They have long been recognized in the field of optics and photonics for their exceptional infrared transparency and as highly optically nonlinear materials;[12-14] and have found application in diverse forms ranging from optical fibre and thin film to micro/nanoparticles as well as 2D and van der Waals heterostructures.[14-18] They are renowned as phase-change media, with a unique capacity for fast, reversible, non-volatile switching between amorphous and crystalline phases having markedly different properties (of refractive index, resistivity, etc.)[19-21], upon which basis they have been of fundamental scientific interest (in chemistry, physics and materials

science) and technological importance (optical, and more recently electronic, data storage) for many decades.[12, 22, 23]

As phase-change media, chalcogenides have facilitated a range of 'active' nanophotonic and plasmonic metamaterial devices for applications ranging from electro- and all-optical signal switching and polarization modulation to beam steering and multispectral imaging.[23-29]

Lately, the high NIR refractive index and amorphous-crystalline index contrast of germanium antimony telluride (GST) has been harnessed in the realization of laser-rewritable and optically switchable all-dielectric (i.e. all-chalcogenide) metamaterials.[30, 31] At shorter, visible (VIS) wavelengths crystalline GST is metallic (i.e. plasmonic) so the amorphous-crystalline transition here brings about a change in the fundamental character of the chalcogenide, enabling plasmonic resonances in all-GST metamaterials to be switched 'on' and 'off'.[32]

Bismuth-based chalcogenide alloys, on the other hand, have been shown to present UV to NIR plasmonic properties in both amorphous and polycrystalline thin film form.[33, 34] A variety of bulk monocrystalline bismuth-based chalcogenides have also been recognized as topological insulators (TIs) – semiconductors with topologically-protected metallic surface states arising through strong spin-orbit interactions.[33, 35-37]

In the present study we consider bismuth antimony telluride (Bi:Sb:Te or BST) - an archetypal ternary chalcogenide, along with its binary variants Bi:Te and Sb:Te. Members of this compositional family are variously known as thermoelectric materials[38] and are among those identified recently (in chemically and epitaxially grown monocrystalline form) as TIs.[33, 37, 39, 40] The spectral dispersion of relative permittivity $\varepsilon$ for BST alloys adheres to a generic form consistent with a simple, single Lorentzian oscillator model for semiconductor optical response:[41, 42] the real part $\varepsilon'$ (**Figure 1**) is characteristically large and positive at long (NIR) wavelengths and has a negative minimum value in the VIS-UV range. In consequence, $\varepsilon'$ crosses (i.e. is equal to) zero at some point in the VIS-NIR range, and again in the UV. The specifics of these behaviors – maximum and minimum values of permittivity, zero-crossing

wavelengths, and associated values of $\varepsilon''$, are strong functions of stoichiometry. As such, the alloys present an exceptionally wide and potentially interesting variety of compositionally-adjustable photonic properties: they are typically high-refractive-index dielectrics in the NIR range, plasmonic ($\varepsilon' < 0$) at shorter wavelengths, and low- (including sub-unitary) index / low-epsilon ($\varepsilon' \approx 0$ with low $\varepsilon''$) media in the UV-VIS domain (indeed, some may even be suitable for the manifestation of peculiar 'epsilon-near-zero' electromagnetic wave and light-matter interaction phenomena).[34, 43, 44] We present here a systematic study of optical properties encompassing a large proportion of the BST ternary and Bi/Sb:Te binary range, demonstrating that stoichiometric control can provide an effective means of continuously tuning the UV-NIR optical and plasmonic properties of vapour-deposited chalcogenide thin films.

The compositional space of a ternary alloy system can be rapidly and systematically explored through the synthesis of compositional gradient thin films using combinatorial evaporative physical vapour deposition (ePVD) and high-throughput characterization.[45] Multiple individually atomic sources are configured to co-deposit precisely calibrated density gradients of each elemental component in an ultra-high vacuum environment: Controlled and reproducible compositional gradient alloys are synthesised over a 35x35 mm substrate using fixed 'wedge shutters' which ensure that for every composition, the atomic components are mixing simultaneously. One of the advantages of this method is that the amorphous phases of alloys can be formed directly during synthesis.[46] With composition varying over the substrate, crystallographic, electrical, optical properties can be measured together with film thickness and crystallisation temperature in order to obtain the compositional and structural dependence.

For the present study, thin films of BST (ranging in thickness from 17 to 265 nm) were deposited using a HT-PVD system (**Figure 2a**) equipped with three off-axis Knudsen cell sources (Bi, Sb and Te, each of ≥99.9999% purity) in a 3-fold symmetric arrangement around the target substrate (which is held at room temperature) under $\leq 10^{-8}$ mbar vacuum conditions.

The density gradient of each constituent element over the substrate is independently controlled by setting the position of a 'wedge shutter' that partially shadows the corresponding source, while deposition rate is set by source temperature. The system was calibrated to produce a film (identically on each of several optically flat silicon and sapphire substrates – see Experimental Section) encompassing a large proportion of the BST ternary space and Bi/Sb:Te binaries. The compositional range achieved included 0-55 at.% bismuth, 7−97 at.% antimony, and 3−92 at.% tellurium. The spatial distributions of individual elements, determined by energy dispersive x-ray (EDX) spectroscopy (see Experimental Section) are shown in **Figure 2c**, while the combined compositional spread encompassed in the present study for the optical properties analysis (100 compositions) is shown in **Figure 2b** (note here that while composition varies continuously as a function of position over a substrate, the envelope of synthesized compositions[46] is represented by a set of discrete points corresponding to a 10 × 10 square matrix of positions, with point-to-point separation of 2.1 mm in *x*- and *y*-directions, at which composition was evaluated by EDX spectroscopy). X-ray diffraction (XRD) in conjunction with EDX measurements, reveals that a substantial majority of Bi/Sb:Te binaries compositions are deposited in an amorphous form; instead, as-deposited ternaries are found to be in a (partially) polycrystalline form (see Supporting Information Figures S1-S2).

The spectral dispersion of complex relative permittivity $\varepsilon = \varepsilon' + i\varepsilon''$ (and correspondingly that of refractive index $N = n + i\kappa$) was measured, again over an array of 10 × 10 compositional points, by variable-angle spectroscopic ellipsometry. **Figure 3** shows a representative selection of BST permittivity and refractive index spectra, from which it can be seen that:

- The real part of the refractive index *n* (**Figure 3a** and inset) is characteristically low - close to if not less than 1 (i.e. the refractive index of vacuum) - in the UV spectral range, offering interesting possibilities in low/high-index hybrid photonic (nano)structures;

- $n$ is in contrast characteristically high - reaching values in excess of 11 - at NIR wavelengths, offering promise for telecoms frequency all-dielectric nanophotonic/metamaterial applications;
- Similarly, the extinction coefficient $\kappa$ (**Figure 3b**) is typically lowest at the short UV end of the measured spectral range and increases with wavelength, in some cases across the entire measured VIS to NIR range, in others to a maximum at some point within that range beyond which it then decreases;
- The real part of relative permittivity $\varepsilon'$ (**Figure 3c**) is characteristically equal to zero at an almost compositionally-invariant UV wavelength $\lambda_1$ of around 250 nm; The corresponding imaginary part of relative permittivity $\varepsilon''$ (Figure 3d) typically takes its minimum value for a given composition at or around this point;
- The spectral position $\lambda_2$ of the second $\varepsilon'$ zero-crossing, and thereby the range of wavelengths over which $\varepsilon'$ is negative (i.e. over which an alloy is plasmonic), is a strong function of stoichiometry, as are the associated losses (values of $\varepsilon''$) (Figures 3c and 3d). It should be noted here that the UV-NIR plasmonic properties of BST (and p-block semiconductors in general, i.e. compounds of elements in groups 13 [IIIA] to 18 [VIIIA] of the periodic table, with valence electrons in the p-orbital) differ from those of the noble metals in that they derive not from the excitation of free charges (a mechanism that becomes relevant in such materials only at much longer wavelengths) but rather from the excitation of strong interband transitions, with a possible contribution in some cases from topological conductive surface states.[47]

To look more systematically at some of these behaviours: **Figure 4a** displays $\lambda_2$ – the longer wavelength $\varepsilon' = 0$ point (i.e. the upper limit of the plasmonic, negative $\varepsilon'$ range) as a function of composition. It is seen that this point red-shifts, all the way from 495 nm out to 1685 nm, with decreasing Te content and with increasing Bi content. ($Bi_5Sb_3Te_4$ exhibits the broadest

plasmonic range, from 210 nm (lowest limit of ellipsometer) - 1685 nm,). Comparable trends are manifested, as one might expect, in values of DC resistivity $\rho$ (evaluated via four-point probe measurements - see Experimental Section and Supporting Information Figure S3) which range from $4\times10^{-2}$ to $1\times10^{-4}$ Ω.cm: The largest value of $\rho$ is observed for a relatively low concentration of Bi, close to the binary $Sb_2Te_3$, and values of resistivity decrease with increasing Bi concentration. This trend essentially reflects the extent of the alloys' metallic character, with Bi and Sb being semimetals while Te is a semiconductor with a small band gap (0.32-0.38 eV).

The corresponding values of ε'' shown in **Figure 4b** is lowest for the Te-rich binaries and increasing steeply with decreasing Te and increasing Bi content. Losses, i.e. values of $\varepsilon''$, at the (almost compositionally invariant) UV $\varepsilon' = 0$ wavelength $\lambda_1$ (**Figure 4c**) are uniformly much lower than at $\lambda_2$. They vary only by a factor of two over the entire measured compositional range but again tend to increase with decreasing Te and increasing Bi content. High-tellurium Sb:Te binaries present the lowest values of ε'' where $\varepsilon' = 0$ and as such may be useful in studies of ENZ phenomena at optical frequencies.

**Figure 5** shows the compositional dependence of BST refractive index at NIR telecommunications wavelengths of 1310 and 1550 nm. The real part of the refractive index reaches a value as high as 8 at 1310 nm (**Figure 5a**) in tellurium-rich (>40 at.%), antimony-lean (<50 at.%) alloys containing 10-40 at.% bismuth. Even higher values of $n$ (close to 9) are observed at 1550 nm for ternary compositions containing 10-20 at.% Bi and 20-70 at.% of either Sb or Te (**Figure 5c**). These exceptionally high values of $n$ tend to be accompanied by high values of $\kappa$, however a range of typically (near-)binary compositions is revealed that present still high values of $n$ (around 6-7) with values of $\kappa$ less than 1, which could support strong resonances when structured as all-dielectric metamaterials.

To assess the various alloys manufactured here for their potential in nanophotonic and metamaterial applications we evaluate three different figures of merit: The first, $F_1$,

characterizes a material's ability to support propagating surface plasmon-polaritons (SPPs) at an interface with vacuum and is defined as the SPP dissipation length $d_{SPP} = 1/k''_{SPP}$ ($k''_{SPP}$ being the imaginary part of the SPP wavevector calculated as $k_{SPP} = k_0\sqrt{\varepsilon_{BST}\varepsilon_{air}/(\varepsilon_{BST}+\varepsilon_{air})}$, where $k_0 = \omega/c$ is the free space wavevector) in units of SPP wavelength $\lambda_{SPP} = 2\pi/k'_{SPP}$:[33, 48]

$$F_1 = \frac{d_{SPP}}{\lambda_{SPP}} = \frac{k'_{SPP}}{2\pi k''_{SPP}} \quad (1)$$

The second figure of merit, $F_2$, characterizes a material's ability to support localized surface plasmon resonances (LSPR) in spherical nanoparticles and is defined as the ratio of resonant frequency to width of the resonance line:[49]

$$F_2 = \frac{|\varepsilon'|}{\varepsilon''} \quad (2)$$

The third figure of merit, $F_3$, characterizes a material's ability to support low loss propagating waves within its volume (as an indicator of suitability as a platform for all-dielectric metamaterials supporting high-quality Mie resonances) and is defined as the dissipation length of a transverse electromagnetic wave $d = \lambda_0/4\pi\kappa$[42] in a dielectric with refractive index $N = n + i\kappa$, in units of its wavelength $\lambda = \lambda_0/n$:

$$F_3 = \frac{d}{\lambda} = \frac{n}{4\pi\kappa} \quad (3)$$

These figures of merit (presented as functions of composition and wavelength in Supporting Information videos V1-3), are plotted in **Figure 6** alongside values for the noble metals and a selection of nitrides and conductive oxides considered to be among the most promising alternative plasmonic media,[8, 50, 51, 55] and semiconductors most frequently employed as platforms for all-dielectric metamaterials, reveal that:

- BST chalcogenides are (within the measured compositional range) uniformly better host materials for SPP's - have higher values of $F_1$ (**Figure 6a**) - than titanium nitride

and transparent conductive oxides (specifically aluminium- and gallium-doped zinc oxide, and indium tin oxide) over the UV to NIR spectral range. They are moreover comparable if not superior to gold at wavelengths below 580 nm and silver below 365 nm. Over the entire spectral range of interest here the highest values of $F_1$ (coming within a factor of ~2 of that of Al at around 800-900 nm) are provided by the ternary alloy $Bi_5Sb_3Te_2$.

- In regard to LSPRs, on the basis of $F_2$ (**Figure 6b**), BST alloys are better than silver below ~330 nm, gold below ~512 nm, TiN below ~690 nm, and TCOs below ~1400 nm. $Bi_5Sb_3Te_2$ is again among the best compositions, presenting a value of $F_2$ for UV-VIS wavelengths that is comparable to that of TiN over the NIR range and to TCOs at the upper limit of the spectral range under consideration. It achieves a maximum value of $F_2$ equal to 1.64 at 350 nm, which is more than sufficient to support high quality resonances.[47]
- As a high-index dielectric, BST comes into its own at NIR wavelengths, with values of $F_3$ (**Figure 6c**) exceeding those of TCOs above ~1240 nm. The highest figures of merit are offered by the binary composition $Sb_3Te_8$ – values come within a factor of 2 of those of germanium (at around 700-800nm), though by virtue of losses are much lower than those of silicon.

In summary, from a systematic study enabled by high-throughput physical vapour deposition and characterization techniques, we derive stoichiometric dependences of the spectrally dispersive photonic properties of binary and ternary bismuth antimony telluride (BST) chalcogenide alloys. It is found that as-deposited thin films can be, variously according to composition near-ultraviolet to visible range low-index/low-epsilon and plasmonic materials, and near-infrared high-index dielectrics. They have respective figures of merit sufficiently large as to make them viable material platforms for a range of (nano)photonic, plasmonic and

metamaterial applications. Indeed, plasmonic figures of merit are generally at least comparable to if not higher than those of well-known 'alternative plasmonic' media such as titanium nitride, and in some wavelength bands those of silver and gold. Within the compositional range accessible to the present study: $Bi_5Sb_3Te_2$ is identified as the best plasmonic stoichiometry (highest figures of merit for both propagating and localized surface plasmon modes); NIR refractive indices as high as $n = 11.5$ are found in certain ternaries but $Sb_3Te_8$ presents the highest ratio of refractive index to extinction coefficient (as a figure of merit for high-index dielectric applications); all compositions have a near- or sub-unitary minimum value of refractive index in the UV range (the lowest measured value being $n = 0.7$ at 296 nm for $BiSb_3Te$); $Bi_2Sb_5Te_{18}$ provides a value of epsilon $|\varepsilon|$ that is nearest to zero ($|\varepsilon| = 2.27$ at 230 nm).

Telluride semiconductors (including BST) are susceptible to atmospheric oxidation with prolonged exposure, particularly to humid environments. Here, experimental samples were stored under vacuum but in photonic device applications one would typically protect such media with transparent capping layers (as for example in rewritable optical discs), especially where the plasmonic or topological insulator (i.e. surface) characteristics are important and/or where the chalcogenide will experience elevated temperatures in phase-change switching applications. BST is of course only one member of a large extended family of chalcogenide materials, which remain to be explored for their nanophotonic applications potential. High-throughput combinatorial techniques, as presented here, can enables rapid, systematic surveys of optical, electronic and structural properties, and thereby optimization via compositional design of material characteristics towards specific application requirements.

**Experimental Section**

Thin films of BST were deposited on Si<100> substrates for energy-dispersive x-ray spectroscopy (EDX) and x-ray diffraction (XRD) for determination of composition and phase

state, and on both silicon and sapphire ($Al_2O_3$) substrates for ellipsometric evaluation of optical properties and 4-point probes measurements of sheet resistance. All substrates had dimensions of 34 mm × 34 mm; BST films are deposited over an area 28 mm × 28 mm; Samples were vacuum sealed immediately upon production and between characterization measurements; Analyses are performed over an array of 10 × 10 points within the central 19 mm × 19 mm region (point-to-point separation 2.1 mm).

Film thickness was measured using a stylus profilometer along the external edges of the film and interpolated over the central characterization domain. Variations in thickness over samples are inherent to the process of synthesising films from three off-axis sources with wedge shutters[45, 46], ranging in the present case from a minimum of 17 nm for the binary alloy Bi[11%]:Te[89%] and a maximum of 265 nm for Bi[15%]Sb[5%]Te[80%].

Compositional analyses were performed using an Oxford Instruments INCA EDX system on a JEOL JSM-5910 SEM with an automated stage programmed for the 10 × 10 sampling point array.

XRD was performed on as-deposited films using a Bruker D8 diffractometer equipped with an Incoatec IμS x-ray source (Cu, 1.54059 Å) with an x-ray beam diameter of 0.25 mm. The incident angle used was 8°.

Resistivity was evaluated from a combination of sheet resistance and film thickness measurements. Sheet resistance was measured in 4-point probe (4PP) configuration a on a Signatone probe station, using two Keithley 2636 SourceMeters.

Optical properties were determined by variable angle spectroscopic ellipsometry (VASE) using a J. A. Woollam M2000 ellipsometer covering the spectral range from 210 to 1686 nm with an automated stage programmed for the 10 × 10 sampling point array.

**Supporting Information**

Supporting Information is available from the author.

**Acknowledgements**

This work was supported by the Engineering and Physical Sciences Research Council, UK [grants EP/M009122/1 and EP/N00762X/1], and the Singapore Ministry of Education [MOE2016-T3-1-006].

Received: ((will be filled in by the editorial staff))

Revised: ((will be filled in by the editorial staff))

Published online: ((will be filled in by the editorial staff))

References

[1] N. I. Zheludev, Y. S. Kivshar, *Nat. Mater.* **2012**, *11*, 917.

[2] B. Luk'yanchuk, N. I. Zheludev, S. A. Maier, N. J. Halas, P. Nordlander, H. Giessen, C. T. Chong, *Nat. Mater.* **2010**, *9*, 707.

[3] P. Moitra, Y. Yang, Z. Anderson, I. I. Kravchenko, D. P. Briggs, J. Valentine, *Nat. Photonics* **2013**, *7*, 791.

[4] S. Jahani, Z. Jacob, *Nat. Nanotechnol.* **2016**, *11*, 23.

[5] S. M. Kamali, E. Arbabi, A. Arbabi, A. Faraon, *Nanophotonics* **2018**, *7*, 1041.

[6] A. M. Urbas, Z. Jacob, L. Dal Negro, N. Engheta, A. D. Boardman, P. Egan, A. B. Khanikaev, V. Menon, M. Ferrera, N. Kinsey, C. DeVault, J. Kim, V. Shalaev, A. Boltasseva, J. Valentine, C. Pfeiffer, A. Grbic, E. Narimanov, L. X. Zhu, S. H. Fan, A. Alu, E. Poutrina, N. M. Litchinitser, M. A. Noginov, K. F. MacDonald, E. Plum, X. Y. Liu, P. F. Nealey, C. R. Kagan, C. B. Murray, D. A. Pawlak, Smolyaninov, II, V. N. Smolyaninova, D. Chanda, *J. Opt.* **2016**, *18*, 53.

[7] A. Y. Zhu, A. I. Kuznetsov, B. Luk'yanchuk, N. Engheta, P. Genevet, *Nanophotonics* **2017**, *6*, 452.

[8] G. V. Naik, J. Kim, A. Boltasseva, *Opt. Mater. Express* **2011**, *1*, 1090.

[9] Y. K. Srivastava, M. Manjappa, L. Cong, H. N. S. Krishnamoorthy, V. Savinov, P. Pitchappa, R. Singh, *Adv. Mater.* **2018**, *30*, 1801257.

[10] N. Dabidian, I. Kholmanov, A. B. Khanikaev, K. Tatar, S. Trendafilov, S. H. Mousavi, C. Magnuson, R. S. Ruoff, G. Shvets, *ACS Photonics* **2015**, *2*.

[11] M. I. Stockman, K. Kneipp, S. I. Bozhevolnyi, S. Saha, A. Dutta, J. Ndukaife, N. Kinsey, H. Reddy, U. Guler, V. Shalaev, A. Boltasseva, B. Gholipour, H. N. S. Krishnamoorthy, K. F. Macdonald, C. Soci, N. I. Zheludev, V. Savinov, R. Singh, P. Groß, C. Lienau, M. Vadai, M. L. Solomon, D. R. Barton III, M. Lawrence, J. A. Dionne, S. V. Boriskina, R. Esteban, J. Aizpurua, X. Zhang, S. Yang, D. Wang, W. Wang, T. W. Odom, N. F. Van Hulst, M. Kling, *J. Opt.* **2018**, *20*, 043001.

[12] B. J. Eggleton, B. Luther-Davies, K. Richardson, *Nat. Photonics* **2011**, *5*, 141.

[13] K. B. Borisenko, J. Shanmugam, B. A. O. Williams, P. Ewart, B. Gholipour, D. W. Hewak, R. Hussain, T. Javorfi, G. Siligardi, A. I. Kirkland, *Sci. Rep.* **2015**, *5*, 5.

[14] B. Gholipour, P. Bastock, C. Craig, K. Khan, D. Hewak, C. Soci, *Adv. Opt. Mater.* **2015**, *3*, 635.

[15] A. M. Dubrovkin, B. Qiang, H. N. S. Krishnamoorthy, N. I. Zheludev, Q. J. Wang, *Nat. Commun.* **2018**, *9*.

[16] M. A. Hughes, Y. Fedorenko, B. Gholipour, J. Yao, T. H. Lee, R. M. Gwilliam, K. P. Homewood, S. Hinder, D. W. Hewak, S. R. Elliott, R. J. Curry, *Nat. Commun.* **2014**, *5*, 9.

[17] B. Chen, G. H. ten Brink, G. Palasantzas, B. J. Kooi, *The Journal of Physical Chemistry C* **2017**, *121*, 8569.

[18] C. C. Huang, F. Al-Saab, Y. Wang, J.-Y. Ou, J. C. Walker, S. Wang, B. Gholipour, R. E. Simpson, D. W. Hewak, *Nanoscale* **2014**, *6*, 12792.

[19] S. R. Ovshinsky, *Phys. Rev. Lett.* **1968**, *21*, 1450.

[20] C. C. Huang, B. Gholipour, J. Y. Ou, K. Knight, D. W. Hewak, *Electron. Lett.* **2011**, *47*, 288.

[21] M. Wuttig, N. Yamada, *Nat. Mater.* **2007**, *6*, 824.

[22] M. Wuttig, H. Bhaskaran, T. Taubner, *Nat. Photonics* **2017**, *11*, 465.

[23] N. Raeis-Hosseini, J. Rho, *Materials* **2017**, *10*, 1046.

[24] B. Gholipour, J. Zhang, K. F. MacDonald, D. W. Hewak, N. I. Zheludev, *Adv. Mater* **2013**, *25*, 3050.

[25] A.-K. U. Michel, D. N. Chigrin, T. W. W. Maß, K. Schönauer, M. Salinga, M. Wuttig, T. Taubner, *Nano Lett.* **2013**, *13*, 3470.

[26] Y. G. Chen, T. S. Kao, B. Ng, X. Li, X. G. Luo, B. Luk'yanchuk, S. A. Maier, M. H. Hong, *Opt. Express* **2013**, *21*, 13691.

[27] A. Tittl, A.-K. U. Michel, M. Schaeferling, X. Yin, B. Gholipour, L. Cui, M. Wuttig, T. Taubner, F. Neubrech, H. Giessen, *Adv. Mater.* **2015**, *27*, 4597.

[28] M. Rude, J. Pello, R. E. Simpson, J. Osmond, G. Roelkens, J. J. G. M. van der Tol, V. Pruneri, *Appl. Phys. Lett.* **2013**, *103*, 141119.

[29] H. N. S. Krishnamoorthy, B. Gholipour, N. I. Zheludev, C. Soci, *Adv. Opt. Mater.* **2018**, *6*, 1800332.

[30] Q. Wang, E. T. F. Rogers, B. Gholipour, C.-M. Wang, G. Yuan, J. Teng, N. I. Zheludev, *Nat. Photonics* **2015**, *10*, 60.

[31] A. Karvounis, B. Gholipour, K. F. MacDonald, N. I. Zheludev, *Appl. Phys. Lett.* **2016**, *109*, 051103.

[32] B. Gholipour, A. Karvounis, J. Yin, C. Soci, K. F. Macdonald, N. I. Zheludev, *NPG Asia Mater.* **2018**, *10*, 533.

[33] J. Yin, H. N. S. Krishnamoorthy, G. Adamo, A. M. Dubrovkin, Y. Chong, N. I. Zheludev, C. Soci, *NPG Asia Mater.* **2017**, *9*, e425.

[34] D. Piccinotti, B. Gholipour, J. Yao, K. F. MacDonald, B. Hayden, N. I. Zheludev, *Opt. Express* **2018**, *26*, 20861.

[35] H. Zhang, C.-X. Liu, X.-L. Qi, X. Dai, Z. Fang, S.-C. Zhang, *Nat. Phys.* **2009**, *5*, 438.

[36] J. Zhang, C.-Z. Chang, Z. Zhang, J. Wen, X. Feng, K. Li, M. Liu, K. He, L. Wang, X. Chen, Q.-K. Xue, X. Ma, Y. Wang, *Nat. Commun.* **2011**, *2*, 574.

[37] W. S. Whitney, V. W. Brar, Y. Ou, Y. Shao, A. R. Davoyan, D. N. Basov, K. He, Q. K. Xue, H. A. Atwater, *Nano Lett.* **2017**, *17*, 255.

[38] V. B. Ufimtsev, V. B. Osvensky, V. T. Bublik, T. B. Sagalova, O. E. Jouravlev, *Adv. Perform. Mater.* **1997**, *4*, 189.

[39] Y.-Y. Li, G. Wang, X.-G. Zhu, M.-H. Liu, C. Ye, X. Chen, Y.-Y. Wang, K. He, L.-L. Wang, X.-C. Ma, H.-J. Zhang, X. Dai, Z. Fang, X.-C. Xie, Y. Liu, X.-L. Qi, J.-F. Jia, S.-C. Zhang, Q.-K. Xue, *Adv. Mater.* **2010**, *22*, 4002.

[40] M. Zhao, J. Zhang, N. Gao, P. Song, M. Bosman, B. Peng, B. Sun, C.-W. Qiu, Q.-H. Xu, Q. Bao, K. P. Loh, *Adv. Mater.* **2016**, *28*, 3138.

[41] H. Ibach, H. Luth, *Solid-State Physics*, Springer, 2009.

[42] F. Wooten, *Optical Properties of Solids*, Academic Press, 1972.

[43] D. Piccinotti, B. Gholipour, J. Yao, K. F. MacDonald, B. E. Hayden, N. I. Zheludev, *Adv. Opt. Mater.* **2018**, 1800395.

[44] I. Liberal, N. Engheta, *Nat. Photonics* **2017**, *11*, 149.

[45] S. Guerin, B. E. Hayden, *J. Comb. Chem* **2006**, *8*, 66.

[46] S. Guerin, B. Hayden, D. W. Hewak, C. Vian, *ACS Comb. Sci.* **2017**, *19*, 478.

[47] J. Toudert, R. Serna, *Opt. Mater. Express* **2017**, *7*, 2299.

[48] B. Dastmalchi, P. Tassin, T. Koschny, C. M. Soukoulis, *Adv. Opt. Mater.* **2016**, *4*, 177.

[49] P. R. West, S. Ishii, G. V. Naik, N. K. Emani, V. M. Shalaev, A. Boltasseva, *Laser Photonics Rev.* **2010**, *4*, 795.

[50] P. B. Johnson, R. W. Christy, *Phys. Rev. B* **1972**, *6*, 4370.

[51] K. M. McPeak, S. V. Jayanti, S. J. Kress, S. Meyer, S. Iotti, A. Rossinelli, D. J. Norris, *ACS Photonics* **2015**, *2*, 326.

[52] G. V. Naik, J. L. Schroeder, X. Ni, A. V. Kildishev, T. D. Sands, A. Boltasseva, *Opt. Mater. Express* **2012**, *2*, 478.

[53] G. V. Naik, V. M. Shalaev, A. Boltasseva, *Adv. Mater.* **2013**, *25*, 3264.

[54] D. E. Aspnes, A. A. Studna, *Phys. Rev. B* **1983**, *27*, 985.

[55] W. S. M. Werner, K. Glantschnig, C. Ambrosch-Draxl, *J. Phys. Chem. Ref. Data* **2009**, *38*, 1013.

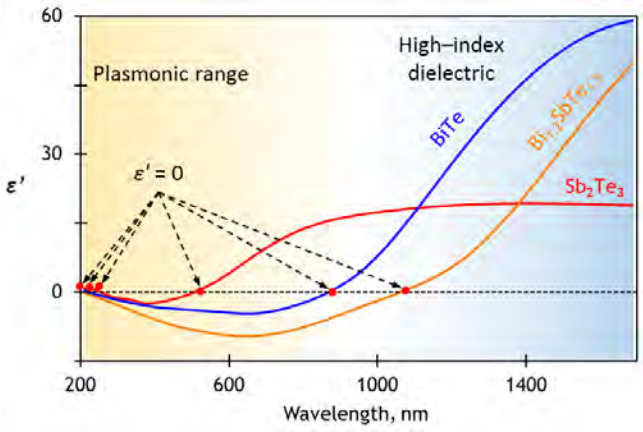


**Figure 1: Permittivity of BST alloys.** Spectral dispersion of the real part of relative permittivity ε' for a representative selection of binary and ternary Bi:Sb:Te chalcogenides.

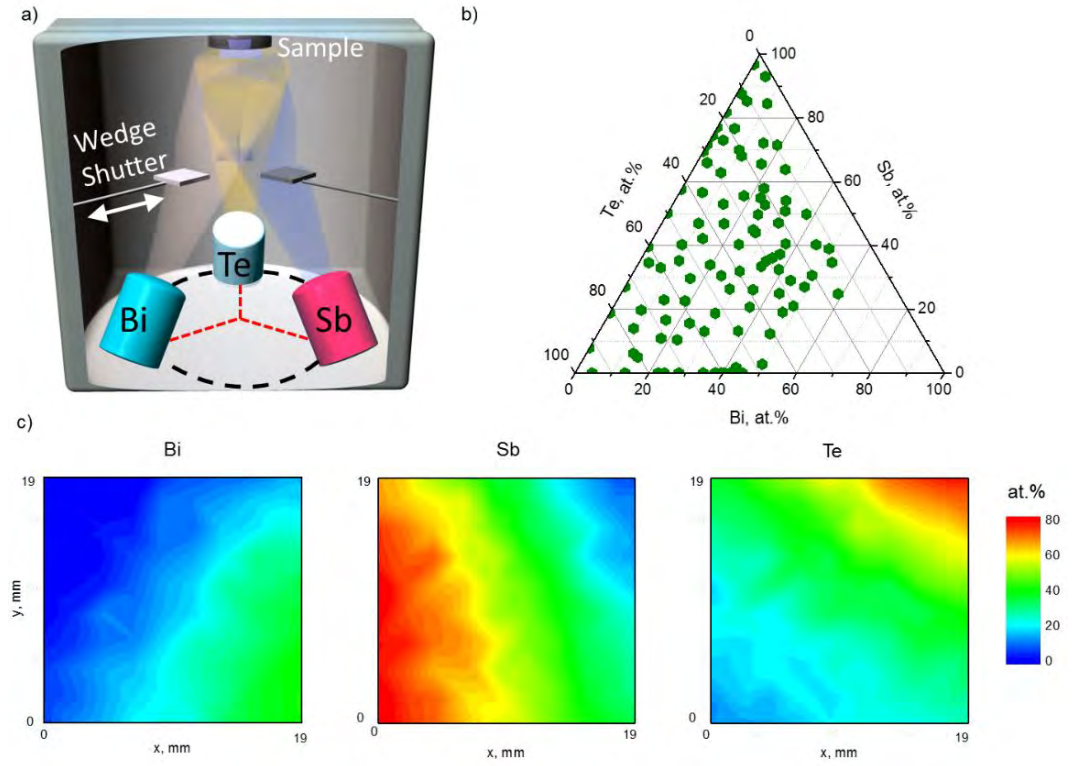


**Figure 2: Combinatorial synthesis of chalcogenide semiconductor thin films.** (a) Schematic of the apparatus for physical vapour deposition of ternary compositional gradient thin BST films, illustrating only the configuration of the most essential components of the ultra-high vacuum system - namely the computer-controlled [K-cell] evaporation sources for each constituent element, 'wedge shutters' [which control the density gradient of each element over the substrate], and the target substrate. b) Compositional ternary plot showing the stoichiometric range encompassed in the present study for the optical properties analysis – each green point denotes the measured elemental ratio at one of the compositional gradient sampling points. (c) Distributions of Bi, Sb and Te over the surface of a representative BST compositional gradient sample, evaluated by energy dispersive x-ray spectroscopy.

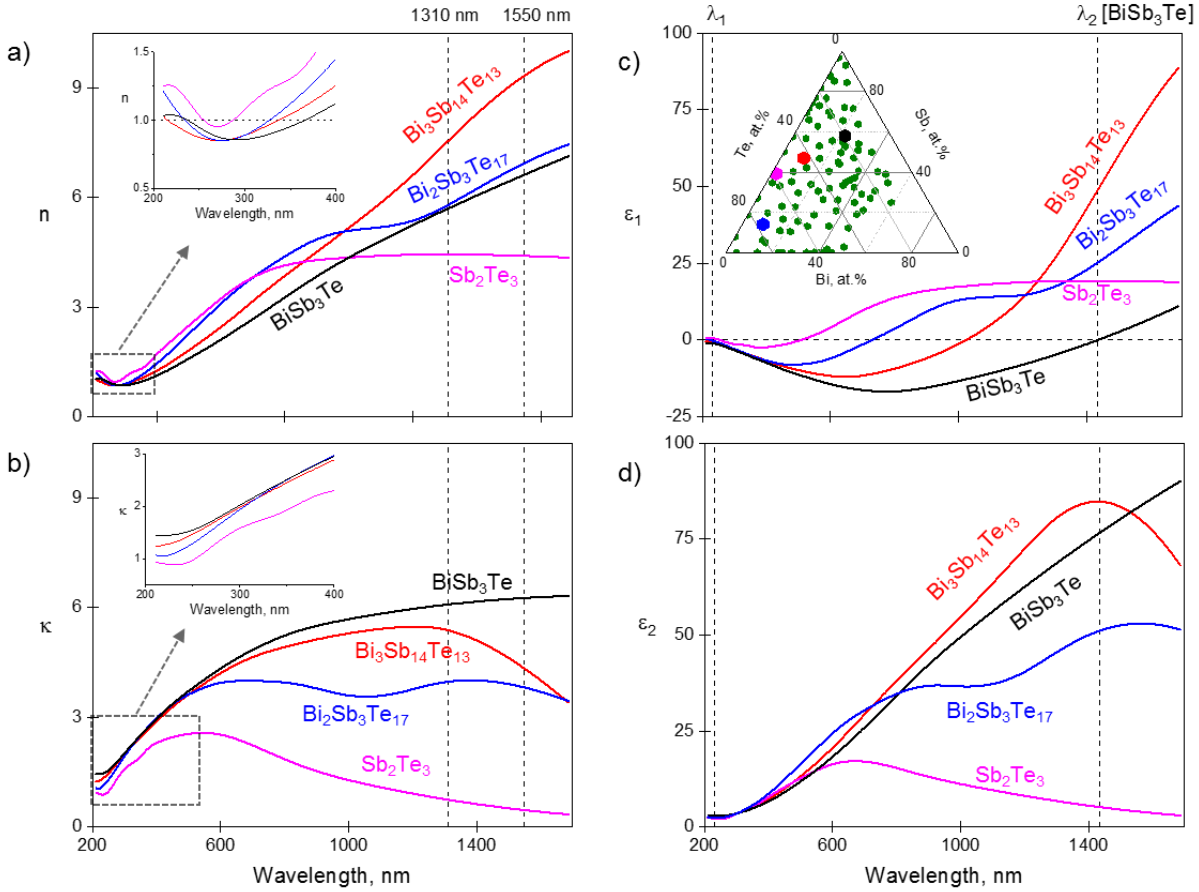


**Figure 3: Compositional variation in spectral dispersion of BST optical properties.**

Spectral dispersion of (a) refractive index *n*, (b) extinction coefficient *κ*, and (c, d) the real and imaginary parts ε' and ε'' respectively of relative permittivity for a selection of BST alloy compositions [as labelled], measured by variable-angle spectroscopic ellipsometry. Insets to (a) and (b) show detail in the 200-400 nm wavelength range. The inset to (c) shows the stoichiometric range encompassed in the present study for the optical properties analysis (100 compositions) – each green point denoting the measured elemental ratio at one of the compositional gradient sampling points; black, red, magenta and blue dots denote the compositions for which spectra are plotted, using lines of the same colour, in the four main panels (a-d).

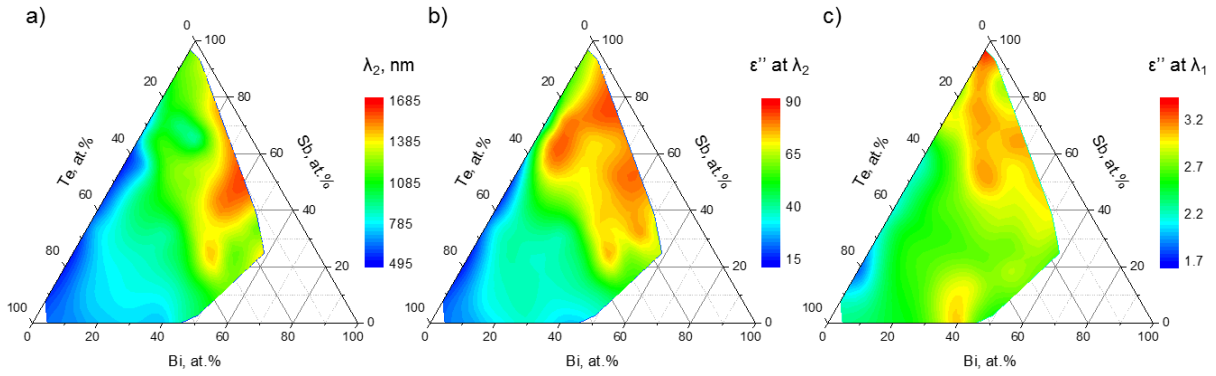


**Figure 4: $\varepsilon' = 0$ properties of BST.** (a) VIS to NIR $\varepsilon' = 0$ wavelength $\lambda_2$, below which an alloy is plasmonic [i.e. has a negative value of $\varepsilon'$] as a function of composition, and (b) the corresponding value of $\varepsilon''$. (c) Compositional dependence of the value of ε'' at the UV $\varepsilon' = 0$ wavelength $\lambda_1$ [~250 nm for all compositions].

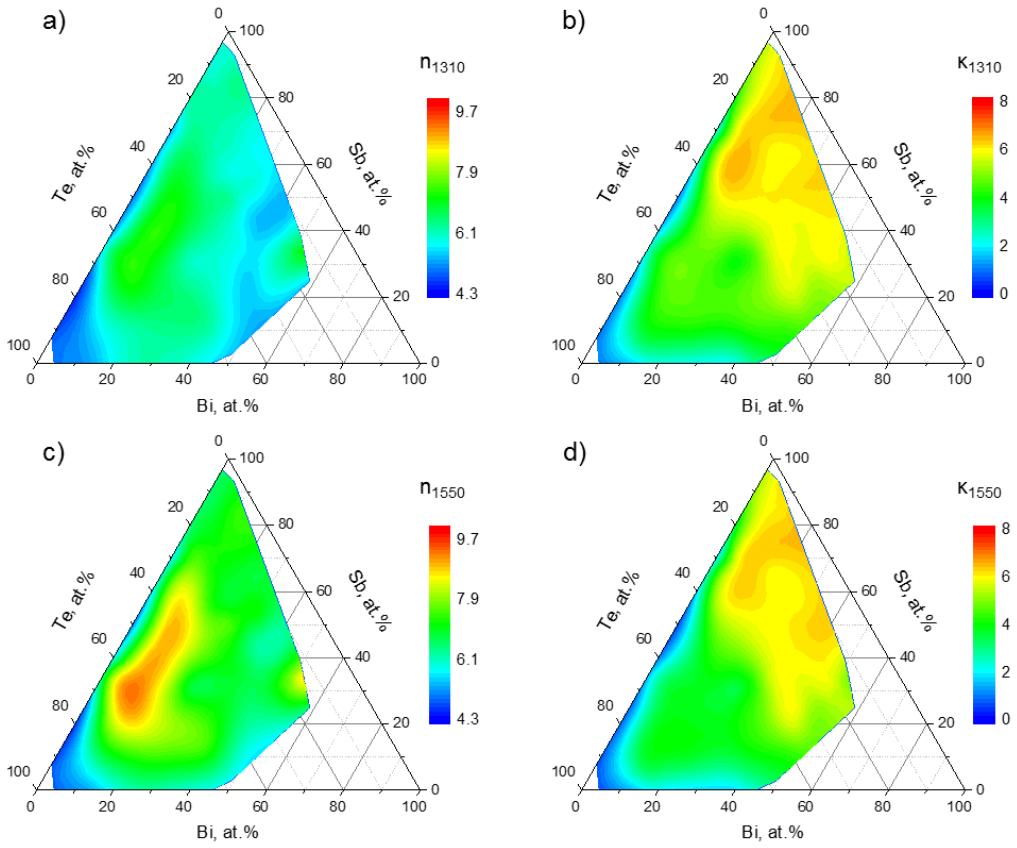


**Figure 5: Optical properties of BST at telecoms wavelengths.** Compositional dependence of (a, c) refractive index *n* and (b, d) extinction coefficient $\kappa$ at (a, b) 1310 and (c, d) 1550 nm.

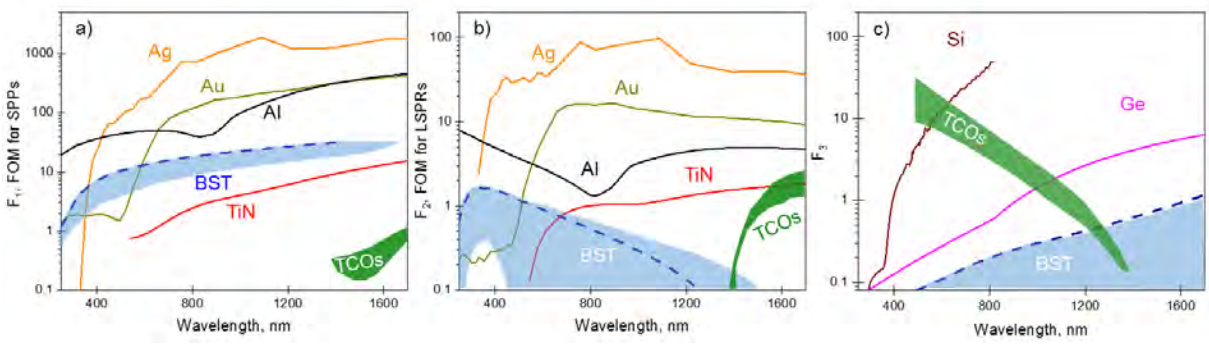


**Figure 6: Performance of BST alloys as plasmonic and high-index dielectric media.** Spectral dispersion of figures of merit [$F_1$, $F_2$, $F_3$] relating to the ability of BST and a selection of other materials [as labelled] to support (a) propagating surface plasmon polaritons at a vacuum interface [$F_1$]; (b) localized, spherical nanoparticle surface plasmons [$F_2$]; (c) low-loss propagating light waves [$F_3$]. Blue areas encompass all ternary and binary BST compositions analysed within the present study [see inset to Fig. 3c]. Dashed blue lines correspond to the particular compositions achieving maximum values of the figures of merit within the UV-NIR spectral range under consideration. Data for other materials is taken from literature as follows: Ag and Au from Ref. [50]; Al from Ref. [51]); TiN from Ref. [52]; TCOs - AZO, GZO and ITO from Ref. [53]; Si from Ref. [54]; Ge optical constants were measured by variable-angle spectroscopic ellipsometry for a Ge film with a thickness of 160 nm deposited by resistive evaporation.

**We explore the plasmonic, epsilon-near-zero, and low/high-index characteristics of Bi:Sb:Te (BST) alloys.** Depending upon composition, they can: present plasmonic figures of merit higher than conductive oxides, nitrides and gold in the UV-VIS range; exhibit dielectric figures of merit better than conductive oxides at telecommunications wavelengths; and achieve record-breaking refractive indices as low as 0.7 and as high as 11.5.

**Keywords:** plasmonics, nanophotonics, metamaterials, chalcogenides, high-throughput

Davide Piccinotti*, Behrad Gholipour*, Jin Yao, Kevin F. MacDonald, Brian E. Hayden and Nikolay I. Zheludev

**Stoichiometric Engineering of Chalcogenide Semiconductor Alloys for Nanophotonic Applications**

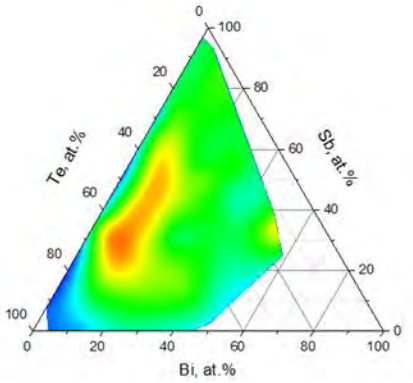

# Supporting Information

## Stoichiometric Engineering of Chalcogenide Semiconductor Alloys for Nanophotonic Applications

*Davide Piccinotti*, Behrad Gholipour*, Jin Yao, Kevin F. MacDonald, Brian E. Hayden and Nikolay I. Zheludev*

### XRD measurements as a function of composition

The XRD measurements mapped to corresponding chemical composition reveals similar features along Te tie-lines of the BST ternary space. Hence, we grouped these XRD spectra in 4 different groups and their corresponding compositions has been plotted in a ternary map labelled by different colours in Figure S1.

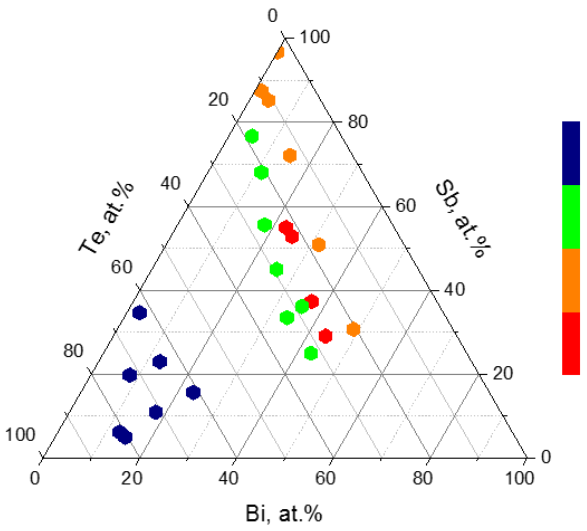


**Figure S1:** Ternary compositional map showing selected compositions grouped along Te tie-lines according to similar features on their corresponding diffractograms.

The actual diffractograms are presented in Figure S2 divided by colours according with Figure S1. The identification of polycrystalline phases from these diffractograms is challenging,[1]

since effects like texturing (defined as the degree to which the crystallites in a polycrystalline film are similarly oriented [2]) can lead to missing Bragg reflections and variations in the relative intensities of the observed peaks compared to conventional powder diffraction.[3] Solid solutions lead to compositionally dependent lattice dimensions, which result in shifting diffraction peaks, and long-range layered structures over the restricted dimension of a thin film make them difficult to identify.[3] Moreover, low energy evaporative PVD synthesis with the substrate at low temperature favours the formation of non-equilibrium phases;[3] hence, the comparison with expected phases reported in literature is not trivial.

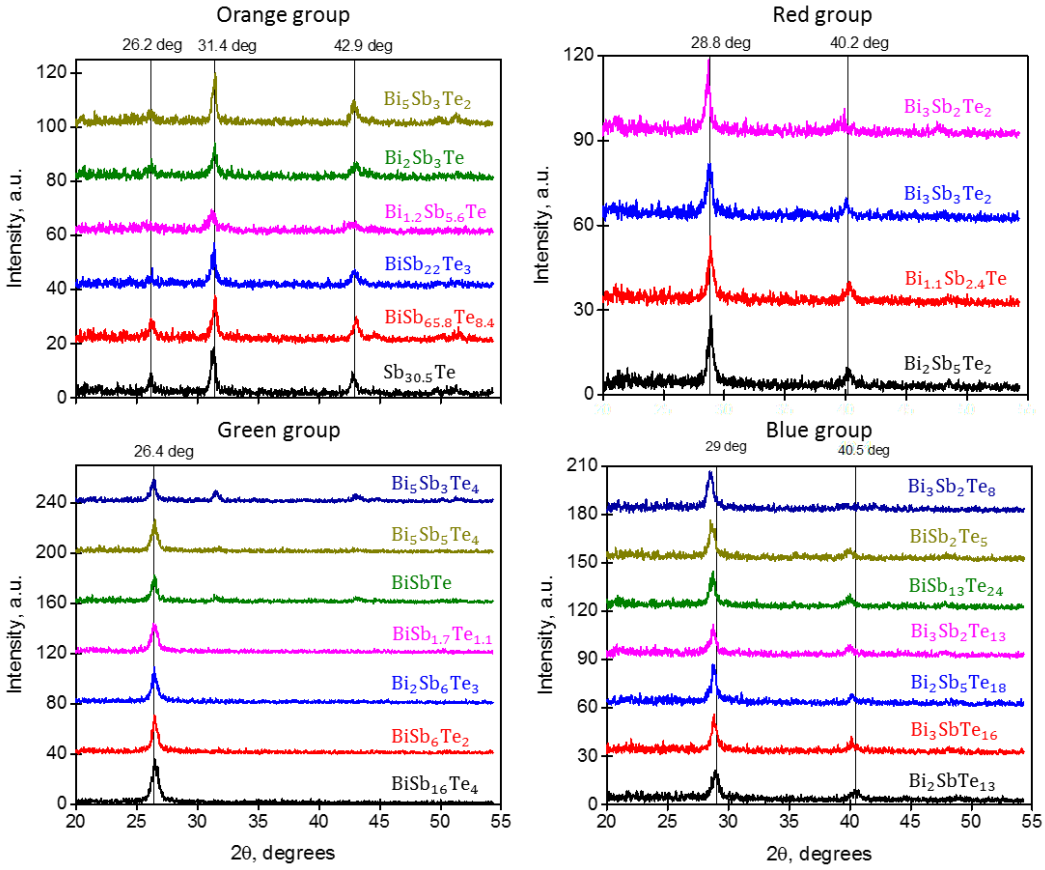


**Figure S2:** XRD diffractograms for selected compositions along Te tie-lines of the BST ternary space. Data are grouped based on similar features visible on the diffractograms. Inside each panel XRD diffractograms are plotted using a vertical offset and are labelled according to the corresponding compositions.

Previous works reported that BST crystallized in a phase belonging to space group $R\bar{3}m$ and is composed of hexagonal close-packed atomic layers which are periodically arranged along the c-axis in five layers.[4-6] A qualitative comparison between literature data and our measured diffractograms suggests that these BST films crystallizes on this phase. We also observe that the peak at 29 degrees for XRD diffractograms of the blue group moves toward smaller angles (2θ) as Te content increases meaning a longer interplanar distance (d) (according to Bragg's law: $2dsin\theta = \lambda$). This is in agreement with reference [7] where they notice that lattice parameters of chalcogenides like $Bi_2Te_3$ rise with Te due to the larger ionic radius of Te.

**Resistivity measurements as a function of composition**

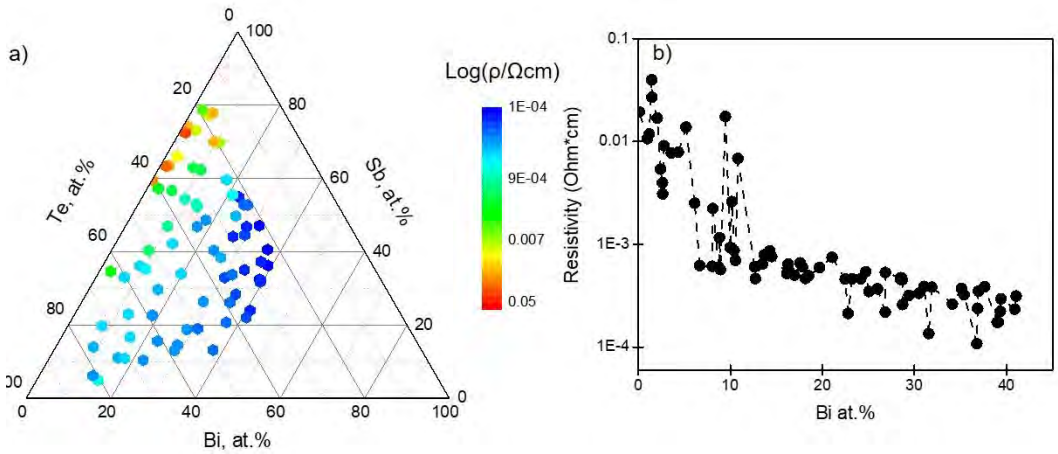


**Figure S3:** a) Resistivity obtained by combining 4-point probe (sheet resistance) and thickness measurements as a function of composition, with corresponding resistivities along the indicated tie-line shown in (b).

**Figures of merit as a function of composition**

Video files V1, V2 and V3 presenting spectral scans of the compositional dependence of figures of merit $F_1$, $F_2$ and $F_3$ respectively.

## References


[1] I. Takeuchi, C. J. Long, O. O. Famodu, M. Murakami, J. Hattrick-Simpers, G. W. Rubloff, M. Stukowski, K. Rajan, *Review of Scientific Instruments* **2005**, *76*.

[2] D. L. Smith, *Thin-Film Deposition: Principles and Practice*, McGraw-Hill Education, 1995.

[3] S. Guerin, B. Hayden, D. W. Hewak, C. Vian, *ACS Comb. Sci.* **2017**, *19*, 478.

[4] W. Richter, H. Kohler, C. R. Becker, *Phys. Status Solidi B* **1977**, *84*, 619.

[5] R. E. Simpson, in *Optoelectronics Research Centre*, Vol. Doctor of Philosophy, University of Southampton, 2008, 245.

[6] W. Liu, L. Endicott, V. A. Stoica, H. Chi, R. Clarke, C. Uher, *Journal of Crystal Growth* **2015**, *410*, 23.

[7] J. Yin, H. N. S. Krishnamoorthy, G. Adamo, A. M. Dubrovkin, Y. Chong, N. I. Zheludev, C. Soci, *NPG Asia Mater.* **2017**, *9*, e425.